

ARTICLE

<https://doi.org/10.1038/s41467-019-11167-z>

OPEN

Observation of two types of charge-density-wave orders in superconducting $\text{La}_{2-x}\text{Sr}_x\text{CuO}_4$

J.-J. Wen ^{1,6}, H. Huang ^{1,6}, S.-J. Lee ^{1,6}, H. Jang ^{1,2}, J. Knight¹, Y.S. Lee^{1,3}, M. Fujita⁴, K.M. Suzuki⁴, S. Asano⁴, S.A. Kivelson⁵, C.-C. Kao¹ & J.-S. Lee ¹

The discovery of charge- and spin-density-wave (CDW/SDW) orders in superconducting cuprates has altered our perspective on the nature of high-temperature superconductivity (SC). However, it has proven difficult to fully elucidate the relationship between the density wave orders and SC. Here, using resonant soft X-ray scattering, we study the archetypal cuprate $\text{La}_{2-x}\text{Sr}_x\text{CuO}_4$ (LSCO) over a broad doping range. We reveal the existence of two types of CDW orders in LSCO, namely CDW stripe order and CDW short-range order (SRO). While the CDW-SRO is suppressed by SC, it is partially transformed into the CDW stripe order with developing SDW stripe order near the superconducting T_c . These findings indicate that the stripe orders and SC are inhomogeneously distributed in the superconducting CuO_2 planes of LSCO. This further suggests a new perspective on the putative pair-density-wave order that coexists with SC, SDW, and CDW orders.

¹SLAC National Accelerator Laboratory, Menlo Park, California 94025, USA. ²PAL-XFEL, Pohang Accelerator Laboratory, Gyeongbuk 37673, South Korea. ³Department of Applied Physics, Stanford University, Stanford, CA 94305, USA. ⁴Institute for Materials Research, Tohoku University, Sendai 980-8577, Japan. ⁵Departments of Physics, Stanford University, Stanford, CA 94305, USA. ⁶These authors contributed equally: J.-J. Wen, H. Huang, S.-J. Lee Correspondence and requests for materials should be addressed to J.-S.L. (email: jslee@slac.stanford.edu)

Since the 1986 discovery¹ of high- T_c superconductivity (SC) in the cuprates, there has been an intense focus on understanding the essential physics of high-temperature SC. A major difficulty arises from the remarkably complex phase diagram. For example, in cuprates there are the so-called pseudogap and strange-metal regimes, and a variety of non-superconducting electronic orders (e.g., density-waves) associated with broken-symmetries^{2–4}. Density wave order can occur on its own, or can coexist with superconducting order^{5–18}. These complexities raise a fundamental question that has yet to be fully addressed—how do these orders/phases interact with SC^{19–21}? Regarding this question, the role of charge-density-wave (CDW) order, which has been observed universally across different families of cuprates^{10–18}, is seemingly the most straightforward to interpret. For instance, in $\text{YBa}_2\text{Cu}_3\text{O}_{6+x}$ (YBCO) the CDW order, which develops above the superconducting T_c , is suppressed with the emergence of SC upon cooling^{12,13}. Conversely, CDW order below T_c is reinforced upon the suppression of the superconducting state by a magnetic field^{22,23}. These phenomena clearly demonstrate a competitive relationship between CDW and SC. Another universally observed electronic order is spin-density-wave (SDW) order^{5–8}, but its relationship with CDW and SC is less clear-cut.

An ideal candidate-material for this study should contain regions in the phase diagram where CDW, SDW, and SC coexist. In YBCO, one of the most-studied cuprates, the experimentally observed CDW and SDW orders appear to be mutually incommensurate, and there is little or no regime in its phase diagram in which these three orders coexist^{24,25}. From a phenomenological perspective, this can be accounted for in terms of a strongly repulsive bi-quadratic coupling in Landau-theory^{26,27}. On the other hand, in the La-based cuprates, $\text{La}_{2-x}\text{y}(\text{Ba,Sr})_x(\text{Nd,Eu})_y\text{CuO}_4$, the CDW and SDW orders tend to satisfy a mutual commensurability condition on the ordering vectors, $q_{\text{cdw}} = 2q_{\text{sdw}}$ ²⁸, which implies the importance of a special tri-linear term in the Landau theory^{26,27}. Moreover, there is generally a range of doping in which all three orders are observed to coexist^{29–32}. In $\text{La}_{2-x}\text{Ba}_x\text{CuO}_4$ (LBCO), $\text{La}_{1.8-x}\text{Eu}_{0.2}\text{Sr}_x\text{CuO}_4$ (LESCO), and $\text{La}_{1.6-x}\text{Nd}_{0.4}\text{Sr}_x\text{CuO}_4$ (LNSCO), however, the phase diagram is further complicated by the existence of a low temperature

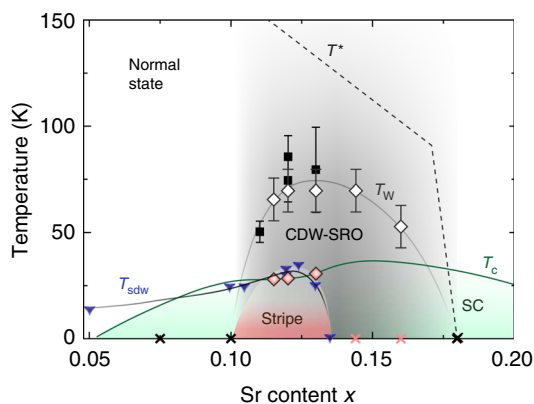


Fig. 1 Phase diagram of LSCO. A sketch of the LSCO phase diagram. The open and filled diamonds denote T_w and the onset temperature of CDW stripe order determined in this study, respectively. The error bar of T_w is estimated to be 10 K. The filled squares are the CDW onset temperature reported in previous X-ray scattering studies^{31,39}. T_{sdw} is the SDW onset temperature determined from neutron scattering measurements^{9,39}. T_c is the superconducting transition temperature³⁹ and T^* is the pseudogap temperature⁴³. The black and red cross symbols indicate the doping levels where no CDW-SRO or CDW stripe order have been detected in this study, respectively

tetragonal (LTT) phase that tends to stabilize the CDW and SDW orders, and depress SC^{28,33}.

In this regard, we view $\text{La}_{2-x}\text{Sr}_x\text{CuO}_4$ (LSCO), which does not undergo LTT transition, as the ideal platform for the present study. As summarized in the schematic phase diagram in Fig. 1, in this study we find a temperature (T) and doping (x) dependence of the CDW order that differs in significant ways from what has been previously conjectured. We reveal distinct behaviors in various ranges of doping: (i) For $x < x_{\text{cdw}} \sim 0.1$ we observe no feature that can readily be identified with CDW order, although neutron scattering and NMR studies reveal the existence of stripe-like SDW order^{9,34,35}. (ii) For $x_{\text{cdw}} \leq x \leq x_{\text{sdw}} \sim 0.135$ we observe CDW order with long correlation length that grows still longer even below superconducting T_c ; from previous studies, x_{sdw} is identified as the upper boundary of the regime in which (quasi) static SDW order persists at low T (with an onset in the neighborhood of T_c)⁹ we identify the growth of CDW correlations below T_c with its mutual commensuration with the SDW order. (iii) For $x_{\text{sdw}} < x < x^* \sim 0.18$, where neutron scattering indicates the existence of a spin-gap at low T and NMR studies show no signatures of quasi-static magnetic order^{9,35}, we still observe clear evidence of well-developed short-range CDW correlations, but these are significantly suppressed at temperatures below T_c . (iv) For $x \geq x^*$, no clear evidence of CDW or SDW order has been observed. In the following sections, detailed experimental findings and their implications will be discussed.

Results

Extending CDW phase diagram of LSCO. The CDW order in LSCO has been observed previously by using X-ray scattering within a limited doping range in the underdoped side ($x = 0.11, 0.12$, and 0.13 , also see Fig. 1)^{31,36–38}. From a detailed analysis of the thermal evolution of the Seebeck coefficient, it was suggested that CDW order is confined to x smaller than a critical doping ~ 0.15 ³⁹. In this context, we first aimed to complete the CDW phase diagram in a wide doping range that extends from the underdoped to the overdoped side ($x = 0.075, 0.10, 0.115, 0.12, 0.13, 0.144, 0.16$, and 0.18). For this purpose, we employed a novel resonant soft X-ray scattering (RSXS) approach that significantly mitigates fluorescence background (see “Methods” section). Figure 2a shows a schematic of how the fluorescence rejection works during the RSXS measurement. A large area detector was used to measure both the signal of interest (near CDW area) and the background signal (away from CDW) simultaneously. By subtracting the background (Fig. 2b, c), we achieve a significantly improved detecting sensitivity in the RSXS, allowing us to explore weak CDW signals. Figure 2d shows the scattering intensity maps along the h - k -direction centered at $q_{\text{cdw}} \sim (-0.23, 0, l)$ r.l.u., which were measured at respective T_c . Clear CDW peaks are observed for $0.1 < x < 0.18$ ($x = 0.115, 0.12, 0.13, 0.144$, and 0.16). Furthermore, in the low dopings we can clearly resolve a CDW peak splitting along the k -direction, which is consistent with previous reports of CDW and SDW coexistence in $x = 0.12$ ^{37,40}. This splitting becomes rather unclear for $x \geq 0.144$, a behavior that seems to be correlated with the disappearance of SDW stripe order above $x_{\text{sdw}} \sim 0.135$ ⁹.

Two types of CDW orders. As a next step, we explore the T dependence of the CDW orders. Figures 3a, b show the projected CDW signals along the h -direction for $x = 0.144$ and 0.13 LSCO, respectively (See Supplementary Fig. 1 for corresponding data for $x = 0.115, 0.12$, and 0.16). Upon cooling, the CDW peak in $x = 0.144$ ($x > x_{\text{sdw}}$) increases, reaching the maximum around T_c , and then decreases as SC emerges below T_c . This is consistent with the expectation that CDW competes with SC^{12,41,42}. For a slightly

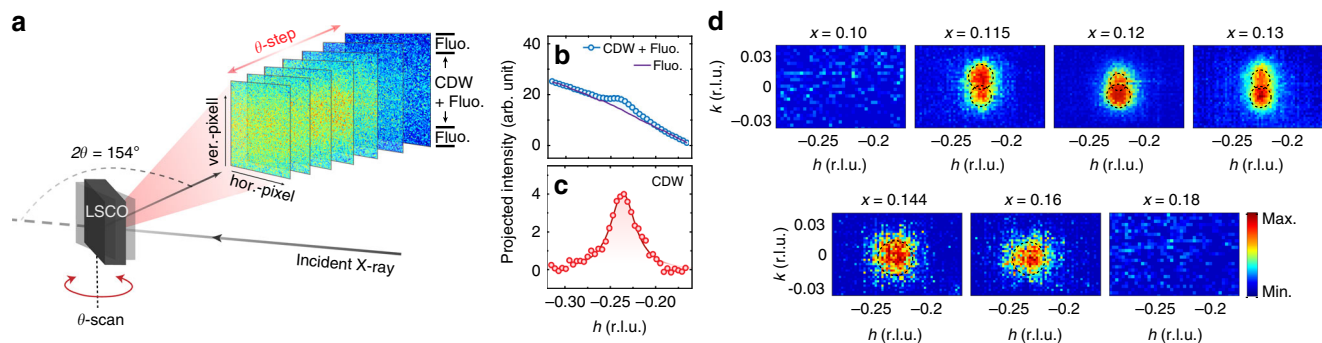


Fig. 2 RSXS measurements on LSCO. **a** A schematic sketch showing the RSXS experimental setup. The top and bottom parts in each CCD image are regarded as the fluorescence (Fluo.) background. **b** The projected intensity profiles along the h -direction at both the CDW area ($k \sim 0$ r.l.u.) and fluorescence area ($k \sim \pm 0.04$ r.l.u.). **c** The CDW profile after subtracting the fluorescence background. The data in **(b)** and **(c)** is for $x = 0.13$ sample measured at 23 K. **d** Scattering patterns for various LSCO samples after subtracting the background. Measurements were taken at respective T_c . The dashed circles outline the intensity contour

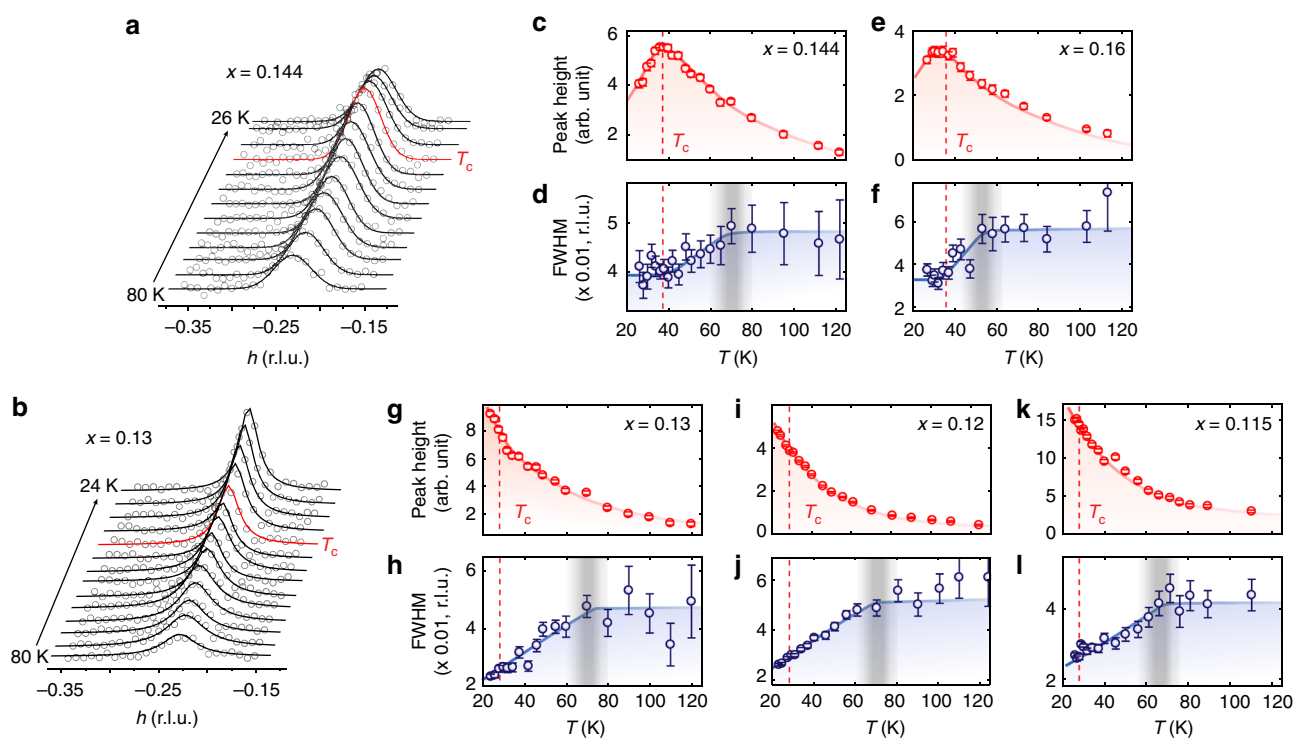


Fig. 3 Temperature dependence of the CDW order in LSCO. **a, b** Projected scattering profiles along h as a function of temperature for $x = 0.144$ **(a)** and 0.13 **(b)** LSCO. The solid lines are Lorentzian fits. The red curves denote the fits for data at T_c . **c–i** Temperature dependent CDW peak heights and full-width at half-maximum (FWHM) extracted from the fits for various LSCO samples. The red dashed lines and vertical gray shades denote T_c and T_w , respectively. The colored shades and lines are guides-to-the-eye. The error bars represent 1 standard deviation (s.d.) of the fit parameters. Source data are provided as a Source Data file

less doped sample of $x = 0.13$ ($x < x_{sdw}$), while the high- T behavior is quite similar, the evolution of the CDW correlations through T_c is surprisingly different. The CDW peak continues to increase with decreasing temperature even below T_c , which has not been unambiguously reported in the previous studies on LSCO^{31,36–38} (Supplementary Discussion and Supplementary Fig. 2).

For quantitative investigation of the T dependence, we fitted the CDW peaks with the Lorentzian function (Fig. 3c–i). For temperatures above T_c , the CDW correlations in all dopings follow similar trend. The peak intensities in all dopings decrease continuously with increasing temperature, showing no clear indication of an onset- T . Notably, the CDW peak intensity in our

study persists even above recent estimates of the pseudogap temperature (T^*) (see Supplementary Fig. 3)⁴³. Instead of an onset- T , we could extract a characteristic temperature (T_w) from the T -dependent full width at half maximum (FWHM) plots. The T_w is the temperature above which the CDW correlation length ξ_{cdw} (calculated as $2/\text{FWHM}$) becomes approximately T -independent and below which the ξ_{cdw} increases with decreasing temperature. Such extracted T_w matches previously reported CDW intensity onset- T as shown in Fig. 1. The T -independent ξ_{cdw} at high temperatures is reasonably short at ~ 24 Å, but is still longer than the CDW wave-length $\lambda_{cdw} \sim 4a \sim 15$ Å. Note that we view $\xi_{cdw} \geq \lambda_{cdw}$ or equivalently $\text{FWHM} \leq q_{cdw}/\pi$, as a minimal condition for unambiguously identifying a diffraction peak as

indicative of CDW order. For temperatures below T_c , clear contrast emerges. For $x > x_{\text{sdw}}$ (Fig. 3c–f), the increasing trend in the ξ_{cdw} stops or even slightly reverses below T_c , which is coincident with the suppression of the CDW peak intensity. This is similar to what is commonly observed in the superconducting YBCO and can be readily explained by the competition between the CDW and the SC^{12,41,42}. Hereinafter, we refer to this as CDW short-range order (SRO). In stark contrast, for $x < x_{\text{sdw}}$ (Fig. 3g–l), both ξ_{cdw} and peak intensity keep increasing below T_c . Such contrast cannot be attributed in any naïve way to enhanced disorder-induced pinning of the CDW-SRO in $x \leq x_{\text{sdw}}$ samples (i.e., $x = 0.115, 0.12$, and 0.13). Given that disorder in LSCO is mainly induced by Sr substitution, these less doped samples are expected, if anything, to have less pinning. This indicates that the enhanced CDW at low- T is a new type of CDW order.

Interplay between the two types of CDW and SDW. To scrutinize this new type of CDW order and the CDW-SRO, we replotted CDW intensities vs. T/T_c for different doping levels with the intensities at T_c normalized to unity (see Fig. 4a). This figure clearly shows two drastically different temperature regimes separated by $T/T_c = 1$. For $T < T_c$, the contrasting behavior of the CDW intensity between $x < x_{\text{sdw}}$ ($x = 0.115, 0.12$, and 0.13 , where static SDW order develops below $\sim T_c$) and $x > x_{\text{sdw}}$ ($x = 0.144$ and 0.16 , where static SDW order is absent) indicates that the enhancement of the CDW order is associated with the development of SDW order. This is further supported by the step-like increase of the low- T CDW correlation length for $x < x_{\text{sdw}}$ as shown in Fig. 4b. Furthermore, the CDW and the SDW in LSCO are found to follow the $q_{\text{cdw}} \sim 2q_{\text{sdw}}$ relation (see Supplementary Fig. 4), which is analogous to the prototypical stripe order in LBCO³⁰. We therefore identify the new type of CDW as the CDW stripe order. For $T > T_c$, the normalized CDW intensities for all doping levels track each other, suggesting that the CDW orders above T_c are of the same short-range-order type. These observations, in conjunction with the fact that neither of the two CDW types exists at doping levels $x = 0.1$ and below even though clear SDW stripe order exists in these dopings^{9,34}, imply that the CDW stripe order is not simply parasitic to the SDW stripe order, but rather is due to a cooperative interaction between SDW and the preexisting CDW-SRO. In short, these findings provide clear and direct evidence of the intertwining between CDW and SDW orders in LSCO.

Discussion

We now discuss the implications of our results on SC. Previous NMR, μ SR and neutron studies of the magnetic correlations for $x < x_{\text{sdw}}$ have demonstrated that the static SDW order is inhomogeneously distributed in the superconducting CuO_2 plane at $T < T_c$ ^{9,35,44,45}. The linkage between the CDW stripe order and the growth of the SDW order for $x_{\text{cdw}} < x < x_{\text{sdw}}$ and $T < T_c$ implies that they are coincident in the same regions. On the other hand, the CDW-SRO, which is presumably uniformly distributed at high- T , is likely to continue to persist in the rest of the regions where SDW order is absent at low- T , but is suppressed by the development of SC. We illustrate such low- T state in Fig. 5, which represents a CuO_2 plane consisting of regions of uniform d -wave SC and regions with the stripe orders. This is the sort of structure expected when two-phase coexistence is frustrated either by disorder or long-range interactions^{3,4}, and is consistent with recent numerical studies that find near degeneracy between SC and stripe state^{46,47}. This picture also provides a plausible explanation for the seemingly contradictory CDW results on $x = 0.12$ LSCO, where the CDW peak intensity increases (ref. 36 and this study), decreases³¹, or levels off^{37,38} upon cooling below T_c . Such

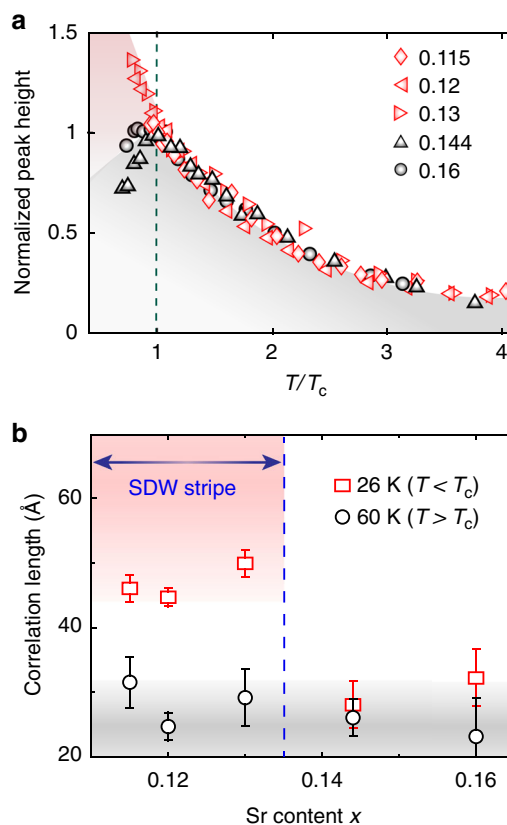


Fig. 4 Comparison of CDW correlations with and without the SDW stripe order in LSCO. **a** Temperature dependent CDW peak heights for $x < x_{\text{sdw}}$ (red) and $x > x_{\text{sdw}}$ (black). Both the peak heights and temperatures are normalized to the values at respective T_c . **b** Doping dependent in-plane CDW correlation length for LSCO samples at 26 K and 60 K. The dashed line denotes the x_{sdw} . The colored shades are guides-to-the-eye. The error bars represent 1 s.d.

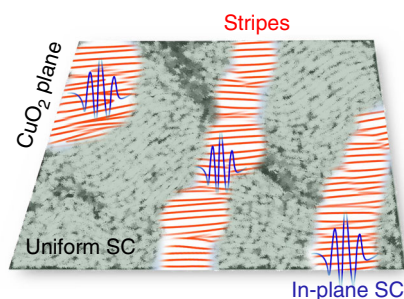


Fig. 5 Inhomogeneous electronic orders in LSCO. Artistic illustration of the stripe-ordered CuO_2 plane in LSCO. The green colored area denotes the uniform SC state. The distorted big-waves illustration indicates the weakened CDW-SRO. Red colored pattern illustrates the stripe orders. The blue modulations formed around the stripe-ordered areas depict the putative PDW

discrepancy can be due to the different volume fractions of CDW stripe order that were probed in different experiments (see “Supplementary Discussion” and Supplementary Fig. 2).

The fact that SDW/CDW stripe order, and SC order all onset at roughly the same T , and that the $SC T_c$ remains sharp implies that these orders are intimately related. In particular, these findings suggest that substantial SC order permeates the stripe-ordered

regions of LSCO. Given that where such stripe order occurs in LSCO, it has been proposed based on transport anomalies that the SC order primarily takes the form of the pair-density-wave (PDW)^{48,49}, it is natural to conjecture that the same is true of the stripe-ordered regions in LSCO. If this is the case, altering the balance between stripe (PDW) ordered and uniform SC regions in CuO₂ plane is expected to affect *c*-axis SC coherence much more dramatically than in-plane SC properties. Indeed, our conjecture is supported by the observation that for $x \sim 0.1$ LSCO, an applied magnetic field much smaller than H_{c2} strongly enhances stripe order⁵⁰ and abruptly quenches *c*-axis SC coherence measured optically⁵¹. Thus the connection between stripe orders and PDW is likely universal in superconducting cuprates beyond LSCO^{48,49}. Future experimental work using a spatially-resolved probe, such as STM, will provide further evidence regarding the spatial distribution of SC order in LSCO. Finally, turning to high T and x , the observation that CDW-SRO persists above T^* , without a change in the correlation length, opens the possibility that it might be directly correlated with other pseudogap phenomena. At minimum, the upper critical doping boundary of the CDW-SRO is strikingly close to the pseudogap critical doping, $x^* = 0.18$ ^{39,43}. Similar correlation has also been noticed in a previous Bi₂Sr₂CaCu₂O_{8+ δ} study⁵².

Methods

Sample preparation. High-quality single crystals of LSCO with nominal concentrations $x = 0.075, 0.10, 0.115, 0.12, 0.13, 0.144, 0.16,$ and 0.18 were grown by the traveling solvent floating zone method. The typical growth rate was 1.0 mm h^{-1} and a 50–60 mm-long crystal rod was successfully obtained for each concentration. A 10 mm-long crystalline piece from the end part of each grown rod was annealed in oxygen gas flow to minimize oxygen deficiencies. Before the RSXS measurements, using a Quantum Design PPMS we characterized their superconducting T_c as the mid-point of the transition. Such obtained T_c for LSCO samples, $x = 0.075, 0.10, 0.115, 0.12, 0.13, 0.144, 0.16,$ and $0.18,$ are 15.0(2), 27.4(2), 27.3(2), 28.4(2), 30.8(2), 37.5(2), 35.5(2), and 30.4(2) K, respectively as summarized in Supplementary Fig. 5.

For the RSXS measurements, we prepared all the samples with a typical dimension of $1.5 \text{ mm} \times 1.5 \text{ mm} \times 2.5 \text{ mm}$ ($a \times b \times c$ axis). To achieve a fresh *c*-axis normal surface, each sample was ex situ cleaved, before transported into the ultra-high vacuum chamber (base pressure = 8×10^{-10} Torr).

RSXS measurement. All the experiments were carried out at beamline 13–3 of the Stanford Synchrotron Radiation Lightsource (SSRL). The sample was mounted on an in-vacuum 4-circle diffractometer. The sample temperature was controlled by an open-circle helium cryostat. Incident photon polarization was fixed as sigma (vertical linear) polarization. Exact ($h, 0, l$) scattering plane was aligned by the measured (0, 0, 2), (−1, 0, 1), and (1, 0, 1) structural Bragg reflections at the photon energy $\sim 1770 \text{ eV}$. The energy of the Cu $L_{2,3}$ -edge was determined by X-ray absorption spectroscopy (see Supplementary Fig. 6). The typical energy resolution of incident X-ray at the Cu L -edge region is 0.1 eV.

A 256×1024 pixel CCD detector was used for the RSXS measurements. Each pixel is of size $26 \mu\text{m} \times 26 \mu\text{m}$. To minimize the geometric effect in the measurements (the background slope as a function of θ -angle), the vertically wide 2D-CCD detector was fixed at $2\theta \sim 154^\circ$ which is the highest achievable 2θ position without blocking incoming X-rays. By rotating the sample (i.e., θ -scan) with 0.5° per step, we obtained the h -dependence. In a typical CDW measurement, each CCD image was accumulated with an exposure time of 3–5 s at each θ . A beam shutter was used to cut the incoming X-ray beam between two consecutive CCD shots to prevent undesired collection of X-ray photons during read-out. In front of the CCD is mounted a 100 nm Parylene/100 nm Al filter to stop electrons emitted from the sample from contributing to CCD signals, ensuring our CCD measures purely X-ray photons. During the θ -scan, each CCD image covers scattering intensities from the well-aligned ($h, 0, l$) scattering plane near the detector center as well as from off-scattering planes ($h, \pm k, l$) at the top/bottom area of the CCD. As described in the main text (Fig. 2a), the scattering intensity near the center of the detector corresponds to the signal of interest (i.e., CDW in this case), while the signals at the off-centered areas are dominated by the fluorescence background. This simultaneously recorded background signal ($\sim 256 \times 50$ pixels near the top and bottom of the CCD detector respectively) was used to subtract out the zeroth order fluorescence contribution near the CDW area. These background regions correspond to $k \sim \pm 0.04 \text{ r.l.u.}$, which is considerably far away from the center of the CDW peak, considering the finite width of the CDW peak.

For data analysis, each CCD pixel was converted to an hkl reciprocal space index, and the resultant three-dimensional scattering intensity data set was projected onto different planes/directions for subsequent analysis.

Data availability

The data that support the findings of this study are available from the corresponding author upon reasonable request.

Received: 27 February 2019 Accepted: 13 June 2019

Published online: 22 July 2019

References

- Bednorz, J. G. & Müller, K. A. Possible high T_c superconductivity in the Ba–La–Cu–O system. *Z. Phys. B* **64**, 189–193 (1986).
- Varma, C. M., Littlewood, P. B., Schmitt-Rink, S., Abrahams, E. & Ruckenstein, A. E. Phenomenology of the normal state of Cu–O high-temperature superconductors. *Phys. Rev. Lett.* **63**, 1996–1999 (1989).
- Emery, V. J. & Kivelson, S. A. Frustrated electronic phase separation and high-temperature superconductors. *Phys. C* **209**, 597–621 (1993).
- Kivelson, S. A., Aeppli, G. & Emery, V. J. Thermodynamics of the interplay between magnetism and high-temperature superconductivity. *Proc. Natl Acad. Sci. USA* **98**, 11903–11907 (2001).
- Tranquada, J. M., Sternlieb, B. J., Axe, J. D., Nakamura, Y. & Uchida, S. Evidence for stripe correlations of spins and holes in copper oxide superconductors. *Nature* **375**, 561–563 (1995).
- Yamada, K. et al. Doping dependence of the spatially modulated dynamical spin correlations and the superconducting-transition temperature in La_{2– x} Sr _{x} CuO₄. *Phys. Rev. B* **57**, 6165–6172 (1998).
- Fujita, M., Goka, H., Yamada, K. & Matsuda, M. Competition between charge- and spin-density-wave order and superconductivity in La_{1.875}Ba_{0.125– x} Sr _{x} CuO₄. *Phys. Rev. Lett.* **88**, 167008 (2002).
- Motoyama, E. M. et al. Spin correlations in the electron-doped high-transition-temperature superconductor Nd_{2– x} Ce _{x} CuO_{4± δ} . *Nature* **445**, 186–189 (2007).
- Kofu, M. et al. Hidden quantum spin-gap state in the static stripe phase of high-temperature La_{2– x} Sr _{x} CuO₄ superconductors. *Phys. Rev. Lett.* **102**, 047001 (2009).
- Abbamonte, P. et al. Spatially modulated ‘Mottness’ in La_{2– x} Ba _{x} CuO₄. *Nat. Phys.* **1**, 155–158 (2005).
- Wu, T. et al. Magnetic-field-induced charge-stripe order in the high-temperature superconductor YBa₂Cu₃O _{y} . *Nature* **477**, 191–194 (2011).
- Ghiringhelli, G. et al. Long-range incommensurate charge fluctuations in (Y,Nd)Ba₂Cu₃O_{6+ x} . *Science* **337**, 821–825 (2012).
- Keimer, B., Kivelson, S. A., Norman, M. R., Uchida, S. & Zaanen, J. From quantum matter to high-temperature superconductivity in copper oxides. *Nature* **518**, 179–186 (2015).
- Comin, R. et al. Charge order driven by Fermi-arc instability in Bi₂Sr_{2– x} La _{x} CuO_{6+ δ} . *Science* **343**, 390–392 (2014).
- Tabis, W. et al. Charge order and its connection with Fermi-liquid charge transport in a pristine high- T_c cuprate. *Nat. Commun.* **5**, 5875 (2014).
- da Silva Neto, E. H. et al. Charge ordering in the electron-doped superconductor Nd_{2– x} Ce _{x} CuO₄. *Science* **347**, 282–285 (2015).
- Jang, H. et al. Superconductivity-insensitive order at $q \sim 1/4$ in electron-doped cuprates. *Phys. Rev. X* **7**, 041066 (2017).
- Hoffman, J. E. et al. A four unit cell periodic pattern of quasi-particle states surrounding vortex cores in Bi₂Sr₂CaCu₂O_{8+ δ} . *Science* **295**, 466–469 (2002).
- Fradkin, E. & Kivelson, S. A. High-temperature superconductivity: ineluctable complexity. *Nat. Phys.* **8**, 864–866 (2012).
- Chen, H.-D., Vafeek, O., Yazdani, A. & Zhang, S.-C. Pair density wave in the pseudogap state of high temperature superconductors. *Phys. Rev. Lett.* **93**, 187002 (2004).
- Lee, P. A. Amperean pairing and the pseudogap phase of cuprate superconductors. *Phys. Rev. X* **4**, 031017 (2014).
- Chang, J. et al. Direct observation of competition between superconductivity and charge density wave order in YBa₂Cu₃O_{6.67}. *Nat. Phys.* **8**, 871 (2012).
- Gerber, S. et al. Three-dimensional charge density wave order in YBa₂Cu₃O_{6.67} at high magnetic fields. *Science* **350**, 949–952 (2015).
- Haug, D. et al. Neutron scattering study of the magnetic phase diagram of underdoped YBa₂Cu₃O_{6+ x} . *New J. Phys.* **12**, 105006 (2010).
- Jang, H. et al. Coincident onset of charge-density-wave order at a quantum critical point in underdoped YBa₂Cu₃O _{x} . *Phys. Rev. B* **97**, 224513 (2018).
- Zachar, O., Kivelson, S. & Emery, V. Landau theory of stripe phases in cuprates and nickelates. *Phys. Rev. B* **57**, 1422 (1998).
- Nie, L., Maharaj, A. V., Fradkin, E. & Kivelson, S. A. Vestigial nematicity from spin and/or charge order in the cuprates. *Phys. Rev. B* **96**, 085142 (2017).
- Tranquada, J. M. Spins, stripes, and superconductivity in hole-doped cuprates. *AIP Conf. Proc.* **1550**, 114–187 (2013).

29. Daou, R. et al. Linear temperature dependence of resistivity and change in the fermi surface at the pseudogap critical point of a high- T_c superconductor. *Nat. Phys.* **5**, 31 (2009).
30. Hückler, M. et al. Stripe order in superconducting $\text{La}_{2-x}\text{Ba}_x\text{CuO}_4$ ($0.095 \leq x \leq 0.155$). *Phys. Rev. B* **83**, 104506 (2011).
31. Croft, T., Lester, C., Senn, M., Bombardi, A. & Hayden, S. Charge density wave fluctuations in $\text{La}_{2-x}\text{Sr}_x\text{CuO}_4$ and their competition with superconductivity. *Phys. Rev. B* **89**, 224513 (2014).
32. Hunt, C. R. et al. Two distinct kinetic regimes for the relaxation of light-induced superconductivity in $\text{La}_{1.675}\text{Eu}_{0.2}\text{Sr}_{0.125}\text{CuO}_4$. *Phys. Rev. B* **91**, 020505 (2015).
33. Achkar, A. et al. Nematicity in stripe-ordered cuprates probed via resonant x-ray scattering. *Science* **351**, 576–578 (2016).
34. Chang, J. et al. Tuning competing orders in $\text{La}_{2-x}\text{Sr}_x\text{CuO}_4$ cuprate superconductors by the application of an external magnetic field. *Phys. Rev. B* **78**, 104525 (2008).
35. Julien, M.-H. Magnetic order and superconductivity in $\text{La}_{2-x}\text{Sr}_x\text{CuO}_4$: a review. *Phys. B* **329**, 693–696 (2003).
36. Wu, H.-H. et al. Charge stripe order near the surface of 12-percent doped $\text{La}_{2-x}\text{Sr}_x\text{CuO}_4$. *Nat. Commun.* **3**, 1023 (2012).
37. Thampy, V. et al. Rotated stripe order and its competition with superconductivity in $\text{La}_{1.88}\text{Sr}_{0.12}\text{CuO}_4$. *Phys. Rev. B* **90**, 100510 (2014).
38. Christensen, N. et al. Bulk charge stripe order competing with superconductivity in $\text{La}_{2-x}\text{Sr}_x\text{CuO}_4$ ($x=0.12$). Preprint at <https://arxiv.org/pdf/1404.3192> (2014).
39. Badoux, S. et al. Critical doping for the onset of fermi-surface reconstruction by charge-density-wave order in the cuprate superconductor $\text{La}_{2-x}\text{Sr}_x\text{CuO}_4$. *Phys. Rev. X* **6**, 021004 (2016).
40. Kimura, H. et al. Incommensurate geometry of the elastic magnetic peaks in superconducting $\text{La}_{1.88}\text{Sr}_{0.12}\text{CuO}_4$. *Phys. Rev. B* **61**, 14366 (2000).
41. Hayward, L. E., Hawthorn, D. G., Melko, R. G. & Sachdev, S. Angular fluctuations of a multicomponent order describe the pseudogap of $\text{YBa}_2\text{Cu}_3\text{O}_{6+x}$. *Science* **343**, 1336–1339 (2014).
42. Nie, L., Sierens, L. E. H., Melko, R. G., Sachdev, S. & Kivelson, S. A. Fluctuating orders and quenched randomness in the cuprates. *Phys. Rev. B* **92**, 174505 (2015).
43. Cyr-Choinière, O. et al. Pseudogap temperature T^* of cuprate superconductors from the Nernst effect. *Phys. Rev. B* **97**, 064502 (2018).
44. Savici, A. T. et al. Muon spin relaxation studies of magnetic-field-induced effects in high- T_c superconductors. *Phys. Rev. Lett.* **95**, 157001 (2005).
45. Imai, T. et al. Revisiting ^{63}Cu NMR evidence for charge order in superconducting $\text{La}_{1.885}\text{Sr}_{0.115}\text{CuO}_4$. *Phys. Rev. B* **96**, 224508 (2017).
46. Corboz, P., Rice, T. M. & Troyer, M. Competing states in the t - j model: Uniform d -wave state versus stripe state. *Phys. Rev. Lett.* **113**, 046402 (2014).
47. Zheng, B.-X. et al. Stripe order in the underdoped region of the two-dimensional Hubbard model. *Science* **358**, 1155–1160 (2017).
48. Li, Q., Hückler, M., Gu, G., Tsvetlik, A. & Tranquada, J. Two-dimensional superconducting fluctuations in stripe-ordered $\text{La}_{1.875}\text{Ba}_{0.125}\text{CuO}_4$. *Phys. Rev. Lett.* **99**, 067001 (2007).
49. Fradkin, E., Kivelson, S. A. & Tranquada, J. M. Colloquium: theory of intertwined orders in high temperature superconductors. *Rev. Mod. Phys.* **87**, 457 (2015).
50. Lake, B. et al. Antiferromagnetic order induced by an applied magnetic field in a high-temperature superconductor. *Nature* **415**, 299 (2002).
51. Schafgans, A. et al. Towards a two-dimensional superconducting state of $\text{La}_{2-x}\text{Sr}_x\text{CuO}_4$ in a moderate external magnetic field. *Phys. Rev. Lett.* **104**, 157002 (2010).
52. Fujita, K. et al. Simultaneous transitions in cuprate momentum-space topology and electronic symmetry breaking. *Science* **344**, 612–616 (2014).

Acknowledgements

We thank John M. Tranquada, Mark P. M. Dean, Stephen Hayden, and J. C. Séamus Davis for insightful discussions. All soft X-ray experiments were carried out at the SSRL (beamline 13–3), SLAC National Accelerator Laboratory, supported by the U.S. Department of Energy, Office of Science, Office of Basic Energy Sciences under Contract No. DE-AC02-76SF00515. J.W. and Y.S.L. acknowledges the support by the Department of Energy, Office of Science, Basic Energy Sciences, Materials Sciences and Engineering Division, under contract DE-AC02-76SF00515. S.A.K. acknowledges the support by Department of Energy, Office of Basic Energy Sciences, under contract no. DE-AC02-76SF00515 at Stanford. M.F. is supported by Grant-in-Aid for Scientific Research (A) (Grant No. 16H02125) and Scientific Research (C) (Grant No. 16K05460).

Author contributions

J.W., H.H., S.L., H.J., J.K., and J.-S.L. carried out the RSXS experiment and analyzed the data. M.F., K.S., and S.A. synthesized the materials. J.W., H.H., S.L., Y.S.L., F.M., S.A.K., C.-C.K., and J.-S.L. wrote the manuscript with input from all authors. J.-S.L. coordinated the project.

Additional information

Supplementary Information accompanies this paper at <https://doi.org/10.1038/s41467-019-11167-z>.

Competing interests: The authors declare no competing interests.

Reprints and permission information is available online at <http://npng.nature.com/reprintsandpermissions/>

Peer review information: *Nature Communications* thanks the anonymous reviewer(s) for their contribution to the peer review of this work. Peer reviewer reports are available.

Publisher's note: Springer Nature remains neutral with regard to jurisdictional claims in published maps and institutional affiliations.



Open Access This article is licensed under a Creative Commons Attribution 4.0 International License, which permits use, sharing, adaptation, distribution and reproduction in any medium or format, as long as you give appropriate credit to the original author(s) and the source, provide a link to the Creative Commons license, and indicate if changes were made. The images or other third party material in this article are included in the article's Creative Commons license, unless indicated otherwise in a credit line to the material. If material is not included in the article's Creative Commons license and your intended use is not permitted by statutory regulation or exceeds the permitted use, you will need to obtain permission directly from the copyright holder. To view a copy of this license, visit <http://creativecommons.org/licenses/by/4.0/>.

© The Author(s) 2019